Published in "Physical Chemistry Chemical Physics 15(8): 2829-2835, 2013"
which should be cited to refer to this work.

Jahn–Teller instability in cationic boron and carbon buckyballs B_{80}^+ and C_{60}^+: a comparative study†

Jules Tshishimbi Muya,[a] Harry Ramanantoanina,[b] Claude Daul,[b] Minh Tho Nguyen,[a] G. Gopakumar[c] and Arnout Ceulemans*[a]

This paper investigates the Jahn–Teller effect in the icosahedral cation B_{80}^+ and compares the descent in symmetry with that in C_{60}^+. For both cations the icosahedral ground state is a ^2H_u state, which exhibits a $H \otimes (g \oplus 2h)$ Jahn–Teller instability. A detailed construction of the potential energy surface of B_{80}^+ using different DFT methods including B3LYP/6-31G(d), VWN/6-31G(d), PBE/TZP and PBE/6-31G(d) shows that, contrary to C_{60}^+, which prefers D_{5d} symmetry, the ground state of B_{80}^+ adopts S_6 point group symmetry. A D_{3d} structure is identified as a saddle point among the S_6 minima of B_{80}^+. The distortion of D_{3d} to S_6 in B_{80}^+ is attributed to a superposition of Jahn–Teller and pseudo-Jahn–Teller effects. Imaginary modes, transforming as the g_g representation, which are present in neutral icosahedral B_{80}, form the dominant symmetry breaking active modes. The pronounced difference between the JT effects in the boron and carbon buckyball cations is due to the plasticity of the boron caps. The calculated Jahn–Teller stabilization of B_{80}^+ is nearly 1549 cm^{-1} (PBE/TZP), which exceeds the stabilization of 596 cm^{-1} computed for C_{60}^+ at the same level.

1. Introduction

Since the prediction of the existence of a B_{80} boron buckyball,[1] computational investigations on the electronic and geometric structures of boron allotropes have been intensified.[2–12] Several fundamental questions remain however unanswered, ranging from methodology to structure prediction. Chen *et al.*[13] searched for the most reliable DFT functional for the treatment of boron nanostructures. For small boron clusters, the PBE functional was found to provide better results than the popular hybrid B3LYP functional.[13] For larger structures it is still unknown as to whether boron will adopt fullerene-like hollow cage structures, such as the buckyball,[1] or on the contrary prefer compact, layered structures, such as core–shell clusters[12] based on an inner B_{12} icosahedron.

In view of the persistent lack of experimental measurements on large cage boron clusters, theoretical computational chemistry so far remains the only tool to advance our knowledge of boron allotropes. The boron buckyball is the pivotal structure that connects carbon and boron clusters, and stands out as a paradigm for computational studies. The distinguishing structural feature of the boron buckyball, as compared to the carbon buckyball, is the presence of 20 extra boron atoms, capping the 20 hexagons of the buckyball. These additional B atoms contribute 60 valence electrons, so that the total electron counts in B_{80} and C_{60} are both equal to 240 valence electrons. Chemical bonding,[14] reactivity,[15] magnetic and electrical properties,[16,17] thermodynamic and thermal stability[1,18] of the neutral B_{80} have been compared to the isoelectronic carbon analogue. The physical properties such as electrical conductivity[19] and hydrogen storage ability[20] were proved to be superior. While C_{60} is non-aromatic, B_{80} turns out to be slightly anti-aromatic based on ring currents and nucleus-independent chemical shift (NICS) calculations.[17] A special feature concerns the symmetry of the B_{80} minimum energy structure. Depending on the quantum chemical method used, this is either I_h or slightly distorted to T_h.[21,22] Muya *et al.*[23,24] recently investigated this symmetry breaking in the neutral icosahedral boron buckyball and identified a pseudo-Jahn–Teller (PJT) mechanism, promoting an $I_h \rightarrow T_h$ symmetry lowering. The distortion mode largely coincides with a component of a g_g normal mode, which has an imaginary frequency in I_h. Quite surprisingly, the frontier orbitals, $6h_u$ HOMO and $8t_{1u}$ LUMO, do not play a role in this symmetry lowering. Instead the symmetry

[a] *Department of Chemistry, University of Leuven, Celestijnenlaan 200F, B-3001 Leuven, Belgium. E-mail: arnout.ceulemans@chem.kuleuven.be*
[b] *Department of Chemistry, University of Fribourg, Chemin du Musée 9, CH-1700 Fribourg, Switzerland*
[c] *Max-Planck Institut für Kohlenforschung, Kaiser-Wilhelm-Platz 1, 45470 Mülheim an der Ruhr, Germany*

† Electronic supplementary information (ESI) available.

breaking is triggered by deep excitations, which are localized on the capping atoms and thus are expected to be absent in the carbon buckyball. According to Bersuker,[25] all forms of symmetry breaking in a molecular system with a non-degenerate ground state are due to vibronic interaction matrix elements between occupied and virtual orbitals. These matrix elements are at the basis of vibrational relaxation which can exceed the harmonic force constants, and may give rise to stabilization of lower symmetry configurations. This effect is called the PJT effect. It is more pronounced when the interacting orbitals are closer together in energy. In principle, in systems with a degenerate ground state the PJT and JT effects may occur simultaneously. Separate assignments of the contributions of both are difficult, though. The finding on the JT surface of a minimal energy structure with an unusual symmetry may indicate the presence of a residual PJT effect.

The anionic and cationic states of B_{80} are characterized by degenerate open electronic shells giving rise to Jahn–Teller (JT) instability. This effect will be superimposed on the PJT instability due to the deeper lying excitations, and as a result we expect for both B_{80}^- and B_{80}^+ a combined distortion mechanism, which has no counterpart in C_{60}^- and C_{60}^+.[26,27] The understanding of the properties of the anionic species is important for the elucidation of the potential superconductivity behaviour of fulleride materials.[28] As an example Yan *et al.*[29] studied the covalent and ionic bond in face-centered-cubic K_3B_{80} and Mg_3B_{80} metals. These structures were predicted to have superconductive character which is superior to their homologous carbon fullerides K_3C_{60}[30] and Mg_3C_{60}.[31] The potential energy surface of the anionic icosahedral molecules derives from a $T \otimes h_g$ JT problem, which to first-order has rotational symmetry. For C_{60}^-, Iwahara *et al.*[32] recently performed a comparative study of the vibronic coupling constants from the photon spectrum provided by Wang *et al.*[33] The stabilization energy was found to be 73.6 meV at the B3LYP/cc-pVTZ level and the absolute values of dimensionless vibronic coupling constants for separate modes, calculated by different methods, vary in between 0.1 and 0.5.[32]

Compared to the near-rotational surface in the anionic clusters, the JT effect in the cationic clusters of the type $H \otimes (g_g + 2h_g)$ is expected to give rise to a warped surface with pronounced local minima, favourable for investigation of lower-lying configurations. The ground state of C_{60}^+ was found to belong to D_{5d} symmetry.[27,34] An intermediate D_{2h} structure plays the role of a saddle point connecting extremal D_{3d} and D_{5d} structures. In contrast, a detailed analysis of the HOMO band shape in the photoelectron spectrum of gaseous C_{60} provided evidence for a dynamic JT effect in the ground state of C_{60}^+, and was claimed to indicate tunnelling states between D_{3d} minima.[35] This conclusion was however criticised by Manini and Tosatti,[36] who drew attention to the inconsistency between the size of the supposed tunnelling splitting (230–290 meV) and the small vibrational quantum (32 meV). In this context, we set out to concentrate in the present work on the JT effect in the cationic species B_{80}^+ as compared to C_{60}^+. As indicated, we expect the potential surface of B_{80}^+ to be marked by well defined energy minima, which differentiates from that of C_{60}^+, due to superposition of a PJT effect in the boron cluster.

2. Method

All the geometries reported in the present work are fully optimized using the hybrid functional B3LYP with the following basis sets 6-31G and 6-31G(d), and the generalized gradient functional PBE with triple-zeta Slater-Type Orbitals (STO) plus one polarization function as basis set (TZP). Harmonic frequency calculations are performed at the B3LYP/6-31G and B3LYP/6-31G(d) levels to ensure that the ground state obtained is vibrationally stable. In addition, we reoptimize some geometries at PBE/6-31G(d) and VWN/6-31G(d) levels. The TURBOMOLE 6.3,[37] Gaussian 0.9,[38] and ADF[39] programs are used for this investigation. The ADF and TURBOMOLE programs have the advantage that they can impose average electronic configurations, which facilitates the calculations of systems with degenerate ground states.[40]

The structural heuristic is based on the epikernel principle, which states that the extremum points on the potential energy surface are more favourable to maximal epikernels than to lower ranking epikernels.[41] The lowest subgroup that can be reached by the JT active modes is called the kernel of the distortion space. Intermediate subgroups between the kernel and the parent high-symmetry group in the degenerate origin are the epikernels. The epikernel principle predicts that the symmetry breaking is an 'economic' process, in the sense that it does not destroy more symmetry elements than needed to remove the degeneracy.

The distortion acting in the molecule is obtained from the geometry difference between the highly symmetrical origin and the minimal energy ground state.[42] This distortion vector can also be analysed in terms of normal vibrational modes. The weight contribution of each vibrational mode in the Jahn–Teller distortion vector provides a description of the distortion mechanism.

One electron is removed from the optimized geometry of icosahedral B_{80} to get B_{80}^+. The starting geometry of B_{80}^+ is thus the optimized geometry of the neutral icosahedral boron buckyball, which has 7 imaginary frequencies of $g_g + t_{2u}$ symmetry. Then, this geometry is fully optimized, at first without constraints and secondly with symmetry constraints adopting the maximal epikernel symmetries D_{5d}, D_{3d}, and D_{2h}. Root mean square deviations (rmsd) are calculated to compare the distorted geometries. The active vibrational modes are extracted, and the corresponding weight coefficients are calculated. The gOpenmol,[43] Gaussview,[44] gmolden[45] and Jmol[46] programs are used for visualization.

3. Results

3.1 Potential energy surfaces of B_{80}^+ and C_{60}^+

In Table 1 we list the results of optimizations performed using the B3LYP in D_{5d}, D_{2h} and D_{3d} epikernel symmetries for both buckyballs. There is an important structural difference between

Table 1 Relative energies (RE, kcal mol^{-1}), number of imaginary frequencies (N_i) and mode symmetry representations, lowest imaginary frequencies in cm^{-1} (ν_i), calculated at the B3LYP/6-31G(d) level for B_{80}^+ and C_{60}^+. The RE values in parentheses are from B3LYP/6-31+G(d,p)

	B_{80}^+ at B3LYP/6-31G(d)			C_{60}^+ at B3LYP/6-31G(d)		
	RE	N_i	ν_i	RE	N_i	ν_i
D_{5d}	3.13 (3.54)	$7(e_{1g} + e_{2g} + e_{2u} + a_{2u})$	i166	0.00	0	
D_{3d}	0.46 (0.69)	1 (a_{2g})	i49	0.53	$4(e_{1g} + e_{2g})$	i297
D_{2h}	0.97 (1.29)	3 ($b_{1g} + b_{2g} + b_{3g}$)	i435	0.16	$1(b_{1g})$	i191
S_6	0.00 (0.00)	0	—	—	—	—

both clusters. For B_{80}^+ all three maximal epikernel geometries exhibit imaginary frequencies, indicating the presence of a further symmetry lowering mechanism. Additional optimizations are then launched from the D_{3d} structure, which is characterized by one imaginary frequency of a_{2g} symmetry. This mode is anti-symmetrical with respect to the twofold axes and the dihedral symmetry planes. Activation of this mode will remove these symmetry elements, and reduce the symmetry to the S_6 point group. This appears to be the absolute minimum of the JT surface for the B_{80}^+ cluster. Further optimizations without symmetry constraints eventually converged at a structure with only the reduced C_i symmetry, which was however extremely close to the S_6 energy minimum and may thus be considered identical within computational accuracy.

The total electronic energy of the S_6 ground state B_{80}^+ was calculated at B3LYP/6-31G(d) and B3LYP/6-31+G(d,p) levels and corresponds, respectively, to −1987.32110 and −1987.34631 Hartrees. The ground state is of ^2A_u symmetry. The vibrational frequency analysis shows all frequencies to be real with the lowest frequency located at 114 cm^{-1} (B3LYP/6-31G(d)).

For C_{60}^+ we reproduce a pentagonal ground state found earlier by Manini *et al.*[27] and by Bako *et al.*[34] However, the warping of the JT surface appears to be extremely small, the difference between D_{5d} and D_{3d} being only 0.53 kcal mol^{-1}, unlike in B_{80}^+, where the difference in energy between the D_{5d} and D_{3d} structures amounts to nearly 2.67 kcal mol^{-1} and thus becomes significant. In both buckyballs, the intermediate epikernel D_{2h} has an energy in between those of the D_{5d} and D_{3d}.

The JT stabilisation energies of B_{80}^+ and C_{60}^+ calculated at the PBE/TZP level are provided in Table 2. To calculate the JT stabilization energy, the B_{80} optimized geometry at the B3LYP/6-31G(d) level is used as reference geometry in the computation of B_{80}^+ using general gradient density. The I_h-B_{80}^+ geometry is optimized using the configurational average as implemented in the TURBOMOLE package program by putting equal fractional electrons in each component of the quintet HOMO, $(6h_u)^9$.

Table 2 B_{80}^+ and C_{60}^+ JT stabilization energies in cm^{-1}, calculated at the PBE/TZP level

Sym.	Γ_{el}	B_{80}^+	C_{60}^+
D_{5d}	$^2A_{1u}$	804	596
D_{3d}	$^2A_{1u}$	1378	228
D_{2h}	$^2B_{1u}$	1147	444
S_6	^2A_u	1549	—

Table 3 Total electronic energies (Hartrees) of epikernels D_{5d}, D_{3d}, D_{2h} and S_6 of B_{80}^+ with different methods. Relative energies in cm^{-1} are in parentheses

B_{80}^+	Γ_{el}	B3LYP/ 6-31G(d)	B3LYP/ 6-31+G(d,p)	PBE/ 6-31G(d)	VWN/ 6-31G(d)
D_{5d}	$^2A_{1u}$	−1987.31611 (1096)	−1987.34067 (1237)	−1984.80333 (602)	−1974.37750 (516)
D_{3d}	$^2A_{1u}$	−1987.32036 (163)	−1987.34521 (241)	−1984.80607 (140)	−1974.37945 (88)
D_{2h}	$^2B_{1u}$	−1987.31956 (338)	−1987.34429 (443)	−1984.80492 (393)	−1974.37928 (125)
S_6	^2A_u	−1987.32110 (0)	−1987.34631 (0)	−1984.80671 (0)	−1974.37985 (0)

According to Table 2, the Jahn–Teller stabilization energies for B_{80}^+ are much higher than that for C_{60}^+. Extreme caution must be taken while comparing the JT stabilization energy evaluated using hybrid and pure DFT functionals. The former may benefit from electron delocalization energies, which needs to be corrected by employing for instance the multideterminantal approach.[40] In comparison, the JT stabilisation energy for C_{60}^+ in D_{5d} symmetry, reported by Manini *et al.*,[27] amounts to 573 cm^{-1}. The coupling was found to be stronger among the h_g modes than the g_g modes. Table 3 presents the total electronic energies of epikernels D_{5d}, D_{3d}, D_{2h} and S_6 of B_{80}^+ with different methods and relative energies in cm^{-1}.

In Table 3, the hybrid B3LYP functional overestimates the relative energies whereas the LDA VWN functional tends to underestimate the energies. The GGA functional PBE gives the relative energies in between the LDA and hybrid values. It should be noted that different basis sets are employed for deriving the energy values listed in Table 2 and Table 3 (TZP, 6-31G(d), 6-31+G(d,p)). The adiabatic ionization energies are determined as the differences between the neutral and cationic ground states, and amount to about 6.3 eV for B_{80} and 7.1 eV for C_{60}. The computed ionization energy of C_{60} is in agreement with the ionization energies found in previous experiments. De Vries and co-workers[47] determined the vertical ionization energy of C_{60} at 7.58 eV with an error ranging between −0.02 and 0.04 eV by means of synchrotron radiation and mass spectrometry. Diaz-Tendero *et al.*[48]also reported a single ionization energy of 7.14 eV for Buckminsterfullerene, at the B3LYP/6-31G(d) level.

The instability of the pentagonal epikernel and the additional symmetry lowering to S_6 are characteristic features of B_{80}^+, which are not encountered in C_{60}^+. We attribute this difference to the presence of persistent PJT forces, which also are present in the neutral boron buckyball. The 7 imaginary frequencies in the neutral I_h boron buckyball are transformed as $g_g + t_{2u}$. Of these modes, the g_g mode gives rise to the absolute T_h minimum. Modes of g_g symmetry also take part in the first-order JT effect of an icosahedral fivefold degenerate state, but they only couple to the trigonal distortion. Superposition of PJT and linear JT forces can thus be inferred to strengthen distortion along g_g symmetry coordinates. The symmetries of the imaginary modes in Table 1 lend support for this conclusion. Upon symmetry lowering from I_h to D_{5d} the pseudo-JT modes $g_g + t_{2u}$ subduce to $e_{1g} + e_{2g} + e_{2u} + a_{2u}$,

which are precisely the imaginary modes of the pentagonal epikernel. This confirms that in the pentagonal epikernel there is no quenching of the PJT forces. In contrast, in the D_{3d} configuration of B_{80}^+ only one imaginary mode remains at i49 cm^{-1} and it belongs to the a_{2g} representation. Upon subduction from I_h to D_{3d} the g_g representation splits as $a_{1g} + a_{2g} + e_g$. Hence in this epikernel the PJT forces are already largely incorporated, except for a small remaining component of the g_g distortion, which activates the further reduction to S_6. This point group is the largest common subgroup of D_{3d} and T_h, and thus represents the maximal common epikernel of the linear and pseudo-JT effects.

3.2 Geometries of epikernels of B_{80}^+

As stated above, the main structural difference between the boron and carbon buckyballs is the presence of 20 extra boron atoms, capping the hexagonal faces. The positions of the caps on the spherical surface were the subject of much debate in the search for the presumable real symmetry of the neutral boron buckyball B_{80}. The noticeable plasticity of caps, with respect to *endo*- or *exo*-hedral radial movements, is important in assigning the symmetry point group.

Table 4 presents the radial distances of the cap atoms, measured from the centre of the cage, in the B_{80}^+ optimized geometries constrained to D_{5d}, D_{3d}, D_{2h}, S_6, C_i, and T_h symmetries. Since all structures are centrosymmetric, only 10 cap positions are given. These values should be compared to the values in the minimal energy structure of T_h symmetry in the neutral boron buckyball, with 12 exohedral caps at a radial distance of 3.94 Å and 8 endohedral ones at a radial distance of 3.66 Å. The calculated radial cap distance in I_h-B_{80}^+ is nearly 3.78 Å, this distance is $\sim$0.04 Å longer than that computed in neutral B_{80} at the B3LYP/6-31G(d) level. As shown in Table 4, D_{3d} and its sub-groups S_6 and C_i are characterized by major inward and outward displacements of two and six cap atoms, respectively. While twelve caps in D_{3d} are quite planar, the corresponding caps in S_6 and C_i are divided into two groups of six moving slightly either inward or either outward. The radial distances from caps to the centre of the B_{80}^+ cage in S_6 and C_i configurations differ by very small values from each other. To check the similarity between S_6 and C_i geometries we have computed the root mean square deviation (rmsd) of the optimized B_{80}^+ geometries after suitable alignment. The rmsd value between the two configurations was estimated to be nearly 0.009 Å, and the difference in energy between the two structures amounts to 0.27 kcal mol^{-1} at the B3LYP/6-31+G(d,p) level. These differences are negligible, suggesting the two structures to be identical within computational accuracy.

Table 4 Endohedral and exohedral radial distances of cap atoms of B_{80}^+ isomers in D_{5d}, D_{3d}, D_{2h}, S_6, C_i and T_h symmetries in Å

S	1	2	3	4	5	6	7	8	9	10
D_{5d}	3.79	3.79	3.79	3.79	3.79	3.85	3.85	3.85	3.85	3.85
D_{3d}	3.58	3.78	3.78	3.78	3.78	3.78	3.78	4.01	4.01	4.01
D_{2h}	3.66	3.66	3.66	3.66	3.94	3.94	3.94	3.94	3.96	3.96
S_6	3.58	3.72	3.72	3.72	3.84	3.84	3.84	4.01	4.01	4.01
C_i	3.57	3.73	3.73	3.75	3.81	3.82	3.83	4.00	4.01	4.02
T_h	3.76	3.76	3.76	3.76	3.87	3.87	3.87	3.87	3.87	3.87

The T_h geometry in Table 4 refers to a state of the cationic B_{80}^+, which is obtained by a process of symmetry projection out of the S_6-B_{80}^+ energy minimum. This proceeds as follows: the boron buckyball is placed in the standard Boyle and Parker[49] orientation, with three C_2-axes along the three Cartesian directions and the S_6-axis of the distorted structure in-between. The projection operation is then given by the following orbit:

$$\hat{P} = (\hat{E} + \hat{C}_2^x + \hat{C}_2^y + \hat{C}_2^z)/4 \quad (1)$$

Operating with this projector on the distortion vector will then yield the parent T_h distortion. This cationic state is found to have indeed 8 endohedral and 12 exohedral caps, exactly as in the neutral T_h-B_{80} geometry described by Gopakumar *et al.*,[3] but the corresponding radial displacements are now less pronounced, being 3.76 instead of 3.66 Å for endohedral, and 3.87 instead of 3.94 Å for exohedral caps from the cage centre.

To gain insight into the mechanism of the loss of icosahedral symmetry in the cation boron buckyball, one can inspect the change in the geometry of icosahedral symmetry arising from the multiple vibrational modes that are interacting with the molecular electronic structure as symmetry destroying forces. Based on group theoretical prediction, the destabilization of the electronic state ^2H_u should involve the distortion forces only of representation g_g and h_g. The following paragraph will focus on the symmetry breaking process in B_{80}^+ and identify the distortion mechanisms responsible for the symmetry lowering.

3.3 Distortion vectors and vibrational modes analysis

The distortion vector is defined as the difference between the coordinates of all atoms in the low-symmetry distorted state *versus* the high-symmetry reference state. A vibrational mode analysis involves the calculation of the overlap between the distortion vector and the normalized vibrational mode eigenvectors of the high-symmetry structure. The overlap factors correspond to the weights of the different normal modes to the total distortion. In Table 5 the relative weight values are given for various symmetry lowering processes, as a percentage of the total norm of the distortion vector. In each case the I_h high symmetry reference coordinates and modes refer to the neutral icosahedral boron buckyball. In all cases the active modes are $a_g + g_g + h_g$. The dominant mode is clearly the g_g mode with an imaginary frequency in the neutral icosahedral boron buckyball; there are additional small contributions of $2h_g$ and $3h_g$. The a_g modes are equally small subsidiary contributions which reflect the cage contraction upon oxidation of the buckyball. Additional information for the multimode analysis of the descent in symmetry of B_{80}^+ carried out by a different calculation method is presented in the ESI.† (Tables S1 and S2).

The mean radius of the B_{80}^+ frame compared to the neutral is reduced by about 0.015 Å, while the mean radius of the cap increases with 0.012 Å.

Table 5 Mode analysis of the low-symmetry distortions of B_{80}^+. Contributions of the normal modes are given as a percentage. The extent of the distortion is given as the norm of the distortion vector

Modes	$I_h \rightarrow S_6$	$I_h \rightarrow T_h$	$T_h \rightarrow S_6$	$I_h \rightarrow D_{3d}$	$D_{3d} \rightarrow S_6$
$1a_g$	0.09	0.22	0.01	0.09	0.00
$2a_g$	0.99	3.54	0.05	1.14	0.01
$3a_g$	0.00	0.00	0.00	0.00	0.04
img_g	97	95	98	96	97
$1g_g$	0.15	0.86	0.00	0.06	1.50
$2g_g$	0.01	0.03	0.01	0.01	0.03
$3g_g$	0.00	0.00	0.00	0.00	0.01
$4g_g$	0.06	0.10	0.05	0.05	0.02
$5g_g$	0.03	0.11	0.01	0.01	0.09
$6g_g$	0.02	0.08	0.01	0.02	0.03
$7g_g$	0.00	0.00	0.01	0.00	0.03
$1h_g$	0.06	0.01	0.07	0.12	0.12
$2h_g$	0.72	0.05	0.09	0.86	0.97
$3h_g$	0.47	0.00	0.57	1.09	0.06
$4h_g$	0.02	0.00	0.03	0.04	0.01
$5h_g$	0.03	0.00	0.03	0.03	0.02
$6h_g$	0.00	0.00	0.00	0.00	0.00
$7h_g$	0.00	0.00	0.00	0.00	0.00
$8h_g$	0.07	0.00	0.09	0.11	0.01
$9h_g$	0.01	0.00	0.02	0.02	0.02
$10h_g$	0.01	0.00	0.02	0.02	0.00
$11h_g$	0.01	0.00	0.01	0.01	0.00
Sum	99.97	99.98	98.67	99.95	100
Norm	0.691	0.329	0.608	0.665	0.182

The data in Table 5 allow the two symmetry breaking processes to be probed:

$$\begin{aligned} I_h &\rightarrow D_{3d} \rightarrow S_6 \\ I_h &\rightarrow T_h \rightarrow S_6 \end{aligned} \tag{2}$$

As the results demonstrate, the JT distortion to the D_{3d} epikernel is largely due to the imaginary g_g mode, which is also the dominant mode in the PJT effect in the neutral buckyball. The a_{2g} mode, which activates the further symmetry breaking from the trigonal intermediate state is also identified as a component of the same imaginary g_g mode.

We also explore an alternative symmetry chain *via* the T_h intermediate, with the purpose of identifying the extent of a PJT effect in the cationic buckyball. In a previous study it was established that the PJT activity in the neutral boron buckyball arises from deep excitations, which do not involve the frontier orbitals.[23,24] As a result the cationic cluster, based on the $(h_u)^9$ HOMO configuration, is expected to retain PJT instabilities on top of JT activity. Apparently the imaginary g_g mode is both PJT and JT active.

Under the trigonal symmetry lowering, the fivefold degenerate quintet H-level splits into $A_1 + 2E$. The linear dependence of the energy of the lowest A_1 component along the trigonal distortion in the g_g space is given by:

$$E(A_1) = -\frac{2}{3} F_G Q_{D_{3d}} \tag{3}$$

where F_G stands for the JT force constant of the g-mode, and the trigonal coordinate is a combination:[50]

$$Q_{D_{3d}} = \frac{1}{2\sqrt{6}}\left(3Q_{ga} - \sqrt{5}\left(Q_{gx} + Q_{gy} + Q_{gz}\right)\right) \tag{4}$$

In contrast a tetrahedral distortion splits the quintet into two degenerate levels: $E + T$. The linear energy dependence of both components is given by[50]

$$\begin{aligned} E(E) &= \frac{3}{2\sqrt{6}} F_G Q_{T_h} \\ E(T) &= -\frac{1}{\sqrt{6}} F_G Q_{T_h} \end{aligned} \tag{5}$$

Here the tetrahedral mode coincides with the $g_g a$ component:

$$Q_{T_h} = Q_{g_g a} \tag{6}$$

Clearly the force is maximal for the trigonal distortion, but nevertheless the tetrahedral symmetry breaking already incorporates a significant fraction of the total force. The branching scheme leading to the trigonal $^2A_{1u}$ runs over the tetrahedral ^2T_u state. This means that we should be comparing the $E(T)$ and $E(A_1)$ energy slopes. The corresponding stabilisation energies are proportional to the squares of these slopes. This yields a ratio of 0.444 : 0.166 between the trigonal *versus* tetrahedral stabilisation. The relative importance of these modes may be estimated from the norm of the respective distortion vectors. One obtains from the data in Table 5:

$$\begin{aligned} I_h \rightarrow T_h &: \ 0.329 \\ I_h \rightarrow D_{3d} &: \ 0.665 \end{aligned} \tag{7}$$

This result indicates that the tetrahedral distortion is larger than the relative contribution predicted by the linear JT effect. This provides evidence that PJT forces are active. We may also evaluate the contribution of the tetrahedral intermediate in the path to the absolute minimum.

$$\begin{aligned} I_h \rightarrow T_h &: \ 0.329 \\ T_h \rightarrow S_6 &: \ 0.608 \\ I_h \rightarrow S_6 &: \ 0.691 \end{aligned} \tag{8}$$

Since the $I_h \rightarrow T_h$ and $T_h \rightarrow S_6$ distortion pathways are orthogonal to each other, the length of the total $I_h \rightarrow S_6$ distortion vector is obtained by taking the square root from the sum of the squared norms of the two pathways, as is verified from eqn (8). Clearly, the second pathway, which is a proper JT process, is the dominant distortion.

In Fig. 1 an external view of both the effective pseudo-JT ($I_h \downarrow T_h$) and JT ($T_h \downarrow S_6$) distortion modes in B_{80}^+ is presented.

Contrary to the pseudo-JT force, which is neatly localized on the caps atoms, the JT implies both caps and the frame as illustrated in the figure. Nevertheless, the combination of the two modes yields a strong displacement of caps and a weak displacement of the frame. The distance of frame atoms to the centre of the cage lies in between 4.19 and 4.27 Å, whereas this distance in neutral B_{80} (T_h and I_h) is about 4.26 Å. These displacements are small compared to the displacements of caps illustrated in Table 2. In C_{60}^+ cap atoms are absent, and JT distortions are frame distortions, which result in the lowering of symmetry in an elongation of the sphere along the pentagonal axis.[33]

On some localized caps, the JT and pseudo-JT forces are acting in opposite directions and tend to cancel each other; on other

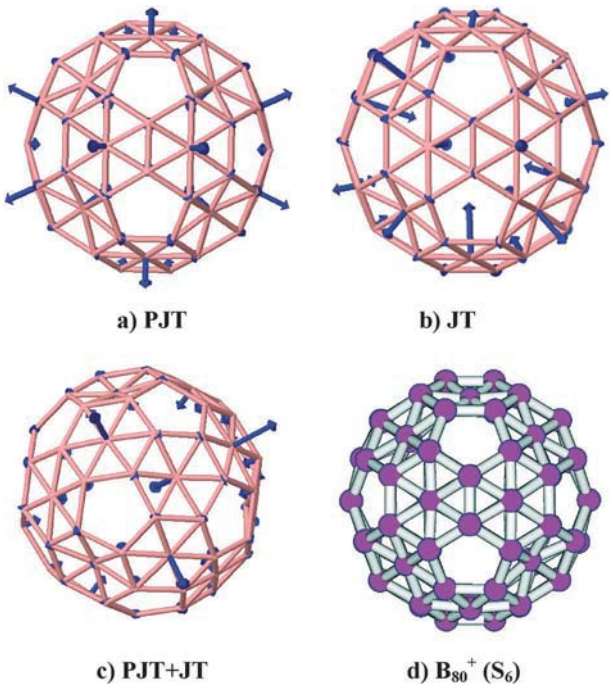

Fig. 1 Distortion vectors in B_{80}^+ and optimization of B_{80}^+ (a) pseudo-JT ($I_h \downarrow T_h$), (b) JT ($T_h \downarrow S_6$), (c) PJT and JT ($I_h \downarrow S_6$) and (d) B_{80}^+ ground state.

atoms the two forces are in the same direction and tend to reinforce the distortion. As a result a distorted molecule is obtained with caps shared in two poles. Each pole contains three caps moving in the exohedral direction of the cage with an amplitude maximum of 0.23 Å and one cap in the middle going inward with maximum displacement amplitude of 0.21 Å, thus forming an improper axis S_6.

4. Concluding remarks

The quintet $H \otimes (g \oplus 2h)$ JT instability[50] was intensively studied for the carbon fullerene cation C_{60}^+ and minima on the potential hypersurface were characterized as D_{5d} wells, connected by D_{2h} saddle points. This is one of the two possible solutions of the standard linear JT problem for the quintet, the other being D_{3d} wells. In B_{80}^+, the plasticity of caps brings an important modification in the symmetry breaking mechanism of icosahedral B_{80}^+. A full geometry optimization at the B3LYP/6-31G(d) level of B_{80}^+ was performed and the frequencies were evaluated to ensure that we have reached the global minima. Our results show that the ground state of B_{80}^+ is outside the three expected epikernel geometries, namely D_{5d}, D_{2h}, and D_{3d}.

Instead its global minimum is characterized by an S_6 symmetry. We attribute this characteristic symmetry to the presence of an additional PJT force, which is also present in the neutral buckyball and is directed towards a tetrahedral distortion. The S_6 group is the largest common sub-group of the D_{3d} JT epikernel and the T_h PJT subgroup.

The ground state geometry of B_{80}^+ distorts slightly from D_{3d} to S_6, keeping the three-fold axis. The resulting S_6 is incompatible with pseudo-JT activity along the t_{2u} imaginary mode present in I_h-B_{80}. The calculated structural relaxation is mainly determined by the plasticity of the caps. This result concurs with the PJT mechanism in the neutral B_{80}.[23,24] Since the PJT in neutral B_{80} is triggered by deeper molecular orbitals, we expect the PJT mechanism in both B_{80} and B_{80}^+ to be originating from exactly the same molecular orbitals.

Acknowledgements

The authors are thankful to the KULeuven Research Council (GOA, ID and DOB programs) and the Swiss National Science Foundation for financial support. JTM is thankful to the Arenberg doctoral School for a scholarship.

References

1 N. G. Szwacki, A. Sadrzadeh and B. I. Yakobson, *Phys. Rev. Lett.*, 2007, **98**, 165.
2 Q. B. Yan, X. L. Shen, Q. R. Zheng, L. Z. Zhang and G. Su, *Phys. Rev. B: Condens. Matter Mater. Phys.*, 2008, **78**, 201401.
3 G. Gopakumar, M. T. Nguyen and A. Ceulemans, *Chem. Phys. Lett.*, 2008, **450**, 175.
4 T. Baruah, M. R. Pederson and R. R. Zope, *Phys. Rev. B: Condens. Matter Mater. Phys.*, 2008, **78**, 045408.
5 D. L. V. K. Prasad and E. D. Jemmis, *Phys. Rev. Lett.*, 2008, **100**, 165504.
6 M. Li, Y. Li, Z. Zhou, P. Shen and Z. Chen, *Nano Lett.*, 2009, **9**, 1944.
7 P. Pochet, L. Genovese, S. De, S. Goedecker, D. Caliste, S. A. Ghasemi, K. Bao and T. Deutsch, *Phys. Rev. B: Condens. Matter Mater. Phys.*, 2011, **83**, 081403.
8 R. R. Zope and T. Baruah, *Phys. Rev. B: Condens. Matter Mater. Phys.*, 2009, **80**, 033410.
9 J. T. Muya, M. T. Nguyen and A. Ceulemans, *Chem. Phys. Lett.*, 2009, **483**, 101.
10 J. L. Li and G. W. Yang, *J. Phys. Chem. C*, 2009, **113**, 18292.
11 J. T. Muya, G. Gopakumar, M. T. Nguyen and A. Ceulemans, *Phys. Chem. Chem. Phys.*, 2011, **13**, 7524–7533.
12 J. Zhao, L. Wang, F. Li and Z. Chen, *J. Phys. Chem. A*, 2010, **114**, 9969.
13 F. Li, P. Jin, D. Jiang, L. Wang, S. B. Zhang, J. Zhao and Z. Chen, *J. Chem. Phys.*, 2012, **136**, 074302.
14 A. Ceulemans, J. T. Muya, G. Gopakumar and M. T. Nguyen, *Chem. Phys. Lett.*, 2008, **461**, 226.
15 J. T. Muya, P. Geerlings, F. De Proft, M. T. Nguyen and A. Ceulemans, *J. Phys. Chem. A*, 2011, **115**, 9069.
16 S. Botti, A. Castro, N. L. Lathiotakis, X. Andrade and M. A. L. Marques, *Phys. Chem. Chem. Phys.*, 2009, **11**, 4523.
17 D. E. Bean, J. T. Muya, P. W. Fowler, M. T. Nguyen and A. Ceulemans, *Phys. Chem. Chem. Phys.*, 2011, **13**, 20855.
18 W. Hayami and S. Otami, *J. Phys. Chem. A*, 2011, **115**, 8204.
19 H. He, R. Pandey, I. Boustani and S. P. Karna, *J. Phys. Chem. C*, 2010, **114**, 4149.
20 M. Olguin, T. Baruah and R. R. Zope, *Chem. Phys. Lett.*, 2011, **514**, 66.

21 N. G. Szwacki and C. J. Tymczak, *Chem. Phys. Lett.*, 2010, **494**, 80.
22 R. N. Gunasinghe, C. B. Kah, K. D. Quarles and X.-Q. Wang, *Appl. Phys. Lett.*, 2011, **98**, 261906.
23 J. T. Muya, G. Gopakumar, E. Lijnen, M. T. Nguyen and A. Ceulemans, in *Vibronic Interactions and the Jahn–Teller Effect: Theory and Applications, Progress in Theoretical Chemistry and Physics*, ed. M. Atanasov *et al.*, Springer, 2011, vol. 23, ch. 14.
24 J. T. Muya, T. Sato, M. T. Nguyen and A. Ceulemans, *Chem. Phys. Lett.*, 2012, **543**, 111.
25 I. B. Bersurker, in *Advances in Quantum Chemistry: Manifestations of Vibronic Coupling in Chemistry and Physics*, ed. J. R. Sabin *et al.*, Elsevier, 2003, vol. 44, p. 6.
26 H. Ramanantoanina, M. Gruden-Pavlovic, M. Zlatar and C. Daul, *Int. J. Quantum Chem.*, 2012, DOI: 10.1002/qua.24080.
27 N. Manini, A. Dal Corso, M. Fabrizio and E. Tosatti, *Philos. Mag. B*, 2001, **81**, 793.
28 T. M. Palstra, *Nat. Mater.*, 2008, **7**, 350.
29 Q. Yan, Q. Zheng and G. Su, *Phys. Rev. B: Condens. Matter Mater. Phys.*, 2009, **80**, 104111.
30 G. Chen, G. Chen, Y. Guo, N. Karasawa and W. A. Goddard III, *Phys. Rev. B: Condens. Matter Mater. Phys.*, 1993, **48**, 13959.
31 C. A. Reed and R. D. Bolskar, *Chem. Rev.*, 2000, **100**, 1075.
32 N. Iwahara, T. Sato, K. Tanaka and L. F. Chibotaru, *Phys. Rev. B: Condens. Matter Mater. Phys.*, 2010, **82**, 245409.
33 X.-B. Wang, H.-K. Woo and L.-S. Wang, *J. Chem. Phys.*, 2005, **123**, 051106.
34 I. Bako, G. Schubert and L. Nemes, *Internet Electron. J. Mol. Des.*, 2003, **2**, 690.
35 S. E. Canton, A. J. Yencha, J. D. Bozek, M. C. Lopes, G. Snell and N. Berrah, *Phys. Rev. Lett.*, 2002, **89**, 045502.
36 N. Manini and E. Tosatti, *Phys. Rev. Lett.*, 2003, **90**, 249601.
37 (*a*) *Turbomole V6.3, a development of Universität Karlsruhe (TH) and Forschungszentrum Karlsruhe GmbH*, 1989–2007, TURBOMOLE GmbH, since 2007; (*b*) R. Ahlrichs, M. Bär, M. Häser, H. Horn and C. Kölmel, *Chem. Phys. Lett.*, 1989, **162**, 165.
38 M. J. Frisch, *et al.*, Gaussian 09, Revision B.01, Gaussian, Inc., Wallingford, CT, 2009.
39 *ADF 2012, SCM, Theoretical Chemistry*, Vrije Universiteit, Amsterdam, The Netherlands, http://www.scm.com.
40 (*a*) R. Bruxndonckx, C. Daul, P. T. Manoharan and E. Deiss, *Inorg. Chem.*, 1997, **36**, 4251; (*b*) H. Ramanantoanina, M. Zlatar, P. Garcia-Fernandez, C. Daul and M. Gruden-Pavlovic, *Phys. Chem. Chem. Phys.*, 2013, **15**, 1252.
41 A. Ceulemans and L. G. Vanquickenborne, *Struct. Bonding*, 1989, **71**, 125.
42 M. Gruden-Pavloviv, P. Garcia-Fernandez, L. Andelkovic, C. Daul and M. Zlatar, *J. Phys. Chem. A*, 2011, **115**, 10801.
43 L. Laaksonen, *J. Mol. Graphics*, 1992, **10**, 33.
44 *GaussView 4.1.2*, Gaussian, Inc., Wallingford, CT, 2004.
45 http://www.cmbi.ru.nl/molden/.
46 *Jmol: an open-source Java viewer for chemical structures in 3D*, http://www.jmol.org/.
47 J. de Vries, H. Steger, B. Kamke, C. Menzel, B. Weisser, W. Kamke and I. V. Hertel, *Chem. Phys. Lett.*, 1992, **188**, 159.
48 S. Diaz-Tendero, G. Sanchez, M. Alcamí and F. Martín, *Int. J. Mass Spectrom.*, 2006, **252**, 133.
49 L. L. Boyle and Y. M. Parker, *Mol. Phys.*, 1980, **39**, 95.
50 A. Ceulemans and P. W. Fowler, *J. Chem. Phys.*, 1990, **93**, 1221.